

Gravity-sensitive Spectral Indices in Ultracool Dwarfs: Investigating Correlations with Metallicity and Planet Occurrence using SpeX and FIRE Observations

FATEMEH DAVOUDI ¹, BENJAMIN V. RACKHAM ^{2,3}, JULIEN DE WIT ², JAN TOOMLAID ², MICHAËL GILLON ¹,
AMAURY H. M. J. TRIAUD ⁴, ADAM J. BURGASSER ⁵ AND CHRISTOPHER A. THEISSEN ⁵

¹*Astrobiology Research Unit, Université de Liège, Allée du 6 Août 19C, B-4000 Liège, Belgium*

²*Department of Earth, Atmospheric and Planetary Science, Massachusetts Institute of Technology, 77 Massachusetts Avenue, Cambridge, MA 02139, USA*

³*Kavli Institute for Astrophysics and Space Research, Massachusetts Institute of Technology, Cambridge, MA, USA*

⁴*School of Physics & Astronomy, University of Birmingham, Edgbaston, Birmingham B15 2TT, UK*

⁵*Department of Astronomy & Astrophysics, University of California San Diego, La Jolla, CA 92093, USA*

ABSTRACT

We present a near-infrared spectroscopic analysis (0.9–2.4 μm) of gravity indices for 57 ultracool dwarfs (M5.5–L0), including exoplanet hosts TRAPPIST-1, SPECULOOS-2, SPECULOOS-3 and LHS 3154. Our dataset includes 61 spectra from the SpeX and FIRE spectrographs. Using gravity-sensitive spectral indices, including FeH absorption (0.99, 1.20, and 1.55 μm), the VO band at 1.06 μm , the H-band continuum, and alkali lines such as K I (1.17 and 1.25 μm), we investigate correlations between surface gravity, stellar metallicity, and the presence of close-in transiting planets. All four planet-hosting stars exhibit intermediate-gravity spectral signatures, despite indicators of field age. However, a volume-corrected logistic regression reveals no significant association between gravity class and planet occurrence. Among individual indices, we find FeH_z to be the most promising tracer of planet-hosting status. We tentatively identify a correlation between FeH_z (0.99 μm) and planet presence at the 2σ level, though the result may reflect observational biases, including transit probability, small-number statistics, and detection sensitivity. More robustly, we find a significant anti-correlation between FeH_z and $[\text{Fe}/\text{H}]$ (3.3σ). A Kruskal–Wallis test shows no significant $[\text{Fe}/\text{H}]$ difference across gravity classes, suggesting the observed FeH_z – $[\text{Fe}/\text{H}]$ trend is not driven by bulk metallicity differences. We propose this anti-correlation may reflect the interplay between age, gravity, and composition: higher-metallicity objects may be systematically younger and have lower gravities, suppressing FeH absorption. While our results only hint at a link between gravity-related characteristics and planet occurrence among late-M dwarfs, they underscore the need for caution when using spectral diagnostics to infer the properties of planet-hosting ultracool dwarfs.

Keywords: Exoplanetary systems; M dwarfs; TRAPPIST-1; SPECULOOS-2; SPECULOOS-3; LHS 3154; techniques: spectroscopic

1. INTRODUCTION

M dwarfs represent the most numerous stellar population in the galaxy, comprising approximately 75% of all stars (Henry et al. 2006, 2018). Their low luminosities—ranging from 100 to 10,000 times less than the Sun—and masses spanning from about 0.61 M_\odot for the hottest types down to the hydrogen-burning limit of 0.075 M_\odot

for the coolest (Henry & Jao 2024), make them essential for studies of stellar formation, evolution, and galactic structure (Reid & Hawley 2005). Additionally, M dwarfs are prime targets for exoplanet searches due to their abundance and the favorable conditions they provide for detecting Earth-sized planets within their habitable zones (Henry & Jao 2024).

Surface gravity significantly influences the atmospheric pressure and temperature profiles of M dwarfs, shaping the strength and morphology of molecular and atomic spectral features. In late-M dwarfs, gravity-

sensitive indicators within the 0.9–2.5 μm spectral range—such as FeH absorption bands (0.99, 1.20, and 1.55 μm), alkali lines including K I (1.17 and 1.25 μm) and Na I (1.14 and 2.21 μm), the VO band at 1.06 μm , and the shape of the H-band continuum—serve as diagnostic tools for youth and low gravity. Lower surface gravity reduces gas pressure in the photospheric layers, leading to weaker FeH and alkali line absorption, enhanced VO band strength, and a characteristic triangular H-band continuum shape (Kleinmann & Hall 1986; Joyce et al. 1998; Meyer et al. 1998; Lucas et al. 2001; Gorlova et al. 2003; McGovern et al. 2004; Allers et al. 2007; Lodieu et al. 2008; Allers & Liu 2013). Expanding on earlier efforts that introduced empirical gravity classifications based on optical alkali and CaH and VO features (Kirkpatrick et al. 2008; Cruz et al. 2009), Allers & Liu (2013) (hereafter AL13) systematically quantified these near-infrared (NIR) features across spectral types M5–L7, enabling the development of gravity indices that quantitatively assess youth in ultracool dwarfs.

While gravity-sensitive spectral indices are well established for young brown dwarfs and field M dwarfs, their interpretation in exoplanet-hosting M dwarfs remains less explored. Intriguingly, some field-age M dwarfs with known planetary systems, such as TRAPPIST-1 and Teegarden’s Star, exhibit spectral signatures commonly associated with youth and low gravity, despite their older estimated ages.

TRAPPIST-1, an M8 dwarf hosting seven terrestrial planets with orbital periods ranging from 1.5 to 18.8 days (Gillon et al. 2017), displays weak FeH absorption and a triangular H-band continuum—traits typically attributed to low gravity (e.g., Gillon et al. 2016; Burgasser & Mamajek 2017). However, TRAPPIST-1 is classified as a field-age star (e.g., Gizis 2002; Filippazzo et al. 2015; Gonzales et al. 2019) with an estimated age of 7.6 ± 2.2 Gyr (Burgasser & Mamajek 2017). Its overall spectral energy distribution also resembles older field stars (Gonzales et al. 2019). Possible explanations for its youth-like spectral features include magnetic activity or tidal interactions with its planets (Gonzales et al. 2019), potentially leading to radius inflation via inhibited convection (MacDonald & Mullan 2017).

A similar ambiguity is seen in Teegarden’s Star, a magnetically inactive M7.5 dwarf at 3.85 pc (Henry et al. 2006; Teegarden et al. 2003). Hosting at least three exoplanets with orbital periods of 4.906, 11.416, and 26.13 days, including two within the conservative habitable zone, it is estimated to be older than 8 Gyr (Zechmeister et al. 2019; Dreizler et al. 2024). Nevertheless, it has been classified as an M7.5 β dwarf, indicating inter-

mediate gravity and youth-like spectral characteristics (Gagné et al. 2015).

These cases raise the possibility that the unusual gravity signatures seen in these ultracool dwarfs may be connected to their planet-hosting status. One explanation is that higher stellar metallicity inflates stellar radii by increasing atmospheric opacity, thereby mimicking low-gravity features and potentially influencing both the star’s spectral appearance and its propensity to form planets. However, metallicity can also directly affect gravity-sensitive features: metal-poor subdwarfs have been shown to exhibit triangular H-band continua and altered FeH absorption that resemble signatures of youth (Aganze et al. 2016; Martin et al. 2017). Similar spectral features have also been reported in $\sim 10\%$ of nearby field-age M dwarfs without known planets (Bardalez Gagliuffi et al. 2019), suggesting an impact from other stellar properties (beyond age or planet occurrence)—or indicating that many nearby M-dwarfs host undetected planets.

While theoretical models predict a decline in super-Earth occurrence toward the lowest-mass stars (Mulders et al. 2021), which agrees with occurrence rates from *K2* (Sestovic & Demory 2020), a global analysis of the TRAPPIST Ultracool Dwarf Transit Survey finds a planet occurrence rate of $\gtrsim 10\%$ for short-period, Earth-sized planets around ultracool dwarfs (Lienhard et al. 2020). Given our generally poor constraints on planet occurrence around late-M dwarfs and the intriguing pattern of low-gravity spectroscopic indicators for detected systems, there exists a notable lack of systematic observational studies directly comparing gravity-sensitive features, metallicity, and planet occurrence within a sample of late-M dwarfs.

To investigate these trends, here we analyze a sample of 57 ultracool M dwarfs spanning spectral types M5.5 to L0, including the known exoplanet hosts TRAPPIST-1, SPECULOOS-2, SPECULOOS-3, and LHS 3154. Using ground-based NIR spectroscopy, we examine gravity-sensitive features to classify each object by gravity regime (high, intermediate, or low) and explore potential correlations with metallicity and planet occurrence. Our aim is to determine whether unusual gravity signatures in planet-hosting late-M dwarfs are linked to underlying physical properties relevant to planet formation and detectability.

This paper is structured as follows. Section 2 describes our sample selection, observations, and data reduction. Section 3 details the computation and analysis of gravity-sensitive indices. Section 4 presents our results and discusses gravity classification in exoplanet-

hosting stars. Finally, [Section 5](#) summarizes our key findings and implications.

2. SAMPLE

We analyze 61 spectra from 57 late-M ultracool dwarfs of spectral types M5.5 to L0 ([Table 1](#)). These targets were selected as part of an ongoing campaign to spectroscopically classify candidates for the SPECULOOS transit survey ([Sebastian et al. 2021](#)). Since our study focuses on gravity-sensitive spectral indices, we limited the sample to field-age stars to avoid confusion with youth-induced low-gravity features. We used the BANYAN Σ tool¹ ([Gagné et al. 2018](#)) to assess kinematic membership in 27 known young associations within 150 pc, excluding all likely members.

2.1. Observations and Data Reduction

Near-infrared spectroscopic observations of our sample were conducted using the SpeX spectrograph ([Rayner et al. 2003](#)) on the 3.2-meter NASA Infrared Telescope Facility (IRTF) at Mauna Kea, Hawaii, and the Folded-port InfraRed Echellette (FIRE) spectrograph ([Simcoe et al. 2013](#)) on the 6.5-meter Magellan Baade Telescope at Las Campanas Observatory, Chile. Of the 61 spectra analyzed, 40 were obtained with SpeX and 21 with FIRE ([Table 1](#)). Except for spectra associated with the exoplanet-hosting stars TRAPPIST-1, SPECULOOS-2, and SPECULOOS-3, none have been previously published.

2.1.1. IRTF/SpeX Near-IR Spectroscopy

SpeX observations were conducted in the short-wavelength cross-dispersed (SXD) mode, covering the 0.8–2.4 μm range at a resolving power of $R \approx 2000$ using the 0.3'' slit. Calibration frames, including dome flat-field frames and ThAr arc lamp spectra, were used to correct pixel-to-pixel sensitivity variations and to perform wavelength calibration. The data were reduced with the SPECTOOL v4.1 pipeline ([Cushing et al. 2004](#); [Vacca et al. 2003](#)), which applies flat-field correction, sky subtraction, spectral extraction, telluric correction, and flux calibration. The sky background was removed by differencing ABBA nodding pairs along the slit, and one-dimensional spectra were extracted from the two-dimensional images. Telluric absorption features were corrected using the xtellcor routine ([Vacca et al. 2003](#)) with A0 V standard stars observed at similar airmasses.

These standards were also used to perform the flux calibration.

2.1.2. FIRE Near-IR Spectroscopy

FIRE observations were conducted in the echellette mode, covering the full 0.8–2.5 μm wavelength range at a resolving power of $R \approx 6000$. The setup included the 0.45'' slit, high-gain mode, and sample-up-the-ramp readout. ABBA nodding along the slit was used to enable sky subtraction. Quartz lamp flats and ThAr lamps were used for flat-field correction and wavelength calibration, respectively. Observations were conducted at airmasses below 1.7 under typical seeing conditions of 0.7'' to 1.1''. Data reduction and spectral extraction were performed using the FIREHOSE pipeline ([Simcoe et al. 2013](#)), which calibrates and combines the echelle orders into one-dimensional spectra. Telluric correction and flux calibration were performed using the xtellcor package ([Vacca et al. 2003](#)) and observations of A0 V standard stars observed at similar airmasses.

2.1.3. A Note on Resolution

To evaluate whether gravity indices are influenced by differences in spectral resolution between SpeX ($R \approx 2000$) and FIRE ($R \approx 6000$), we refer to the findings of [AL13](#). They analyzed low-resolution ($R \approx 100$) and moderate-resolution ($R \approx 750\text{--}2000$) spectra separately and demonstrated that, while one spectral index is less discernible in low-resolution data, their gravity scoring method remains consistent across resolutions. Similarly, [Gonzales et al. \(2019\)](#) analyzed both low- and medium-resolution spectra ($\lambda/\Delta\lambda > 1000$ at the *J*-band) and found gravity class designations to be consistent across resolutions, with only a single outlier. These findings support the reliability of using moderate-resolution spectra for gravity analysis. Given that our spectra fall within the moderate-resolution range ($R \approx 2000\text{--}6000$), they are thus reliable for use in our comparative gravity studies.

2.2. Spectral Classification

SpeX and FIRE spectra of our sample are shown in [Figure 1](#) and [Figure 2](#), respectively. Details for each target—including the instrument used, observation date, near-infrared spectral type, and median signal-to-noise ratio (SNR)—are provided in [Table 1](#). The median per-pixel SNR was calculated over the 8000–24000 Å wavelength range, excluding telluric-dominated regions between 10850–11250 Å and 19000–21000 Å. All spectra in our sample have a median per-pixel SNR > 50 . Each reduced spectrum was visually inspected to confirm the presence and consistency of key ultracool dwarf features.

¹ <https://www.exoplanetes.umontreal.ca/banyan/banyansigma.php>

Table 1. Summary of Spectroscopic Observations and Spectral Types

Object	Instrument	Obs. Date	Spectral Type	SNR (per pixel)
2MASS J00202922+3305081	SpeX	2021/08/30	M5.5V (± 0.5)	62.6
2MASS J00251602+5422547	SpeX	2022/08/12	M6.5V (± 0.5)	72.3
2MASS J02195603+5919273	SpeX	2022/08/12	M5.5V (± 0.5)	96.7
2MASS J02224767-2732349	FIRE	2023/02/01	M6.5V (± 0.5)	95.72
2MASS J03544620+2416246	SpeX	2021/08/30	M6V (± 1.0)	52.8
2MASS J04164276+1310587	SpeX	2021/12/24	M6V (± 1.0)	86.4
2MASS J04333002+5635320	SpeX	2022/02/11	M8V (± 0.5)	67.1
2MASS J04393407-3235516	FIRE	2021/01/07	M6V (± 0.5)	165.0
2MASS J04490464+5138412	SpeX	2022/02/08	M6.5V (± 0.5)	76.9
2MASS J04511406+0305285	FIRE	2021/01/08	M7V (± 1.0)	126.3
2MASS J04511406+0305285	SpeX	2021/12/24	M8V (± 0.5)	43.9
2MASS J04513734-5818519	FIRE	2021/01/07	M6V (± 0.5)	150.0
2MASS J05220976+5754046	SpeX	2022/02/08	M8.5V (± 0.5)	56.6
2MASS J05335379+5054170	SpeX	2022/02/11	M8V (± 0.5)	58.8
2MASS J05512511+5511208	SpeX	2022/02/08	M6V (± 1.0)	77.7
2MASS J06020172-1001565	FIRE	2021/01/08	M6.5V (± 0.5)	141.3
2MASS J06431389+1631428	FIRE	2021/01/08	M7V (± 0.5)	159.6
2MASS J06431389+1631428	SpeX	2021/12/24	M7V (± 0.5)	49.5
2MASS J07552745-2404374	FIRE	2021/01/07	M6.5V (± 0.5)	130.8
2MASS J08055713+0417035	FIRE	2021/01/08	M6.5V (± 0.5)	197.7
2MASS J08055713+0417035	SpeX	2021/12/24	M6V (± 1.0)	90.9
2MASS J08330310+3706083	SpeX	2021/12/24	M8V (± 0.5)	71.1
2MASS J08334323-5336417	FIRE	2021/01/07	M7V (± 0.5)	152.9
2MASS J09332510-4353384	FIRE	2022/06/14	M6V (± 1.0)	103.6
2MASS J09332625-4353366	FIRE	2022/06/14	M6V (± 1.0)	104.2
2MASS J09365564-2609422	SpeX	2022/02/08	M8V (± 0.5)	61.6
2MASS J09432994-3833560	SpeX	2022/02/11	M6V (± 1.0)	79.4
2MASS J10424135-2416050	SpeX	2021/12/24	M6.5V (± 0.5)	25.9
2MASS J10542786-5431322	FIRE	2022/06/14	M6.5V (± 1.0)	85.1
2MASS J11155037-6731332	FIRE	2022/06/14	M8V (± 0.5)	114.0
2MASS J11231964-0509045	SpeX	2022/02/08	M6V (± 0.5)	69.4
2MASS J12294530+0752379	SpeX	2022/02/11	M6.5V (± 0.5)	81.4
2MASS J13273095+0149384	SpeX	2022/02/11	M6.5V (± 0.5)	69.0
2MASS J13313937-6513056	FIRE	2022/06/14	L0 (± 1.0)	76.3
2MASS J14230252+5146303	SpeX	2022/04/19	M7V (± 0.5)	52.3
2MASS J14253465+2540050	SpeX	2022/04/19	M6V (± 0.5)	85.0
2MASS J16105843-0631325	SpeX	2022/07/21	M5.5V (± 0.5)	82.2
2MASS J16210447-3711373	SpeX	2022/04/15	M7V (± 1.0)	60.8
2MASS J17120433-0323300	SpeX	2022/04/19	M6V (± 0.5)	88.7
2MASS J17364180-3425459	FIRE	2022/06/15	M6V (± 1.0)	124.5
2MASS J17415439+0940537	SpeX	2022/07/21	M7V (± 0.5)	67.2
2MASS J18365842-3507176	FIRE	2022/06/15	M6.5V (± 0.5)	74.0
2MASS J18485108-8214422	FIRE	2022/06/14	M7V (± 1.0)	93.4
2MASS J18545092-5704417	FIRE	2022/06/14	M7V (± 1.0)	104.9
2MASS J19212977-2915507	SpeX	2021/08/30	M7V (± 0.5)	89.8
2MASS J19332754+2150009	SpeX	2022/07/21	M8.5V (± 0.5)	51.9
2MASS J19395199-5750339	FIRE	2022/06/14	M6.5V (± 0.5)	67.3
2MASS J19544358+1801581	SpeX	2021/08/30	M8V (± 0.5)	72.4
2MASS J20125255+1246315	SpeX	2021/10/19	M6.5V (± 0.5)	57.1
2MASS J20291194+5750317	SpeX	2021/08/30	M6V (± 0.5)	67.0
2MASS J20495272-1716083	SpeX	2021/10/19	M6.5V (± 0.5)	47.1
2MASS J21010483+0307047	SpeX	2021/10/19	M6.5V (± 0.5)	47.2
2MASS J21265788+2531080	SpeX	2021/08/30	M8.5V (± 0.5)	52.4
2MASS J21381698+5257188	SpeX	2022/08/12	M7V (± 1.0)	66.4
2MASS J21513137-40172297	FIRE	2022/06/14	M7.5V (± 1.0)	116.2
2MASS J22244238+2230425	SpeX	2021/08/30	M6V (± 1.0)	49.7
SPECULOOS-2	SpeX	2021/08/30	M6V(± 0.5)	100.0
SPECULOOS-3	SpeX	2021/08/30	M6.5V(± 0.5)	54.8
LHS 3154	SpeX	2025/04/02	M6V (± 1.0)	64.6

We assigned near-infrared spectral types by comparing each spectrum to those in the IRTF Spectral Library (Cushing et al. 2005; Rayner et al. 2009), focusing on the 0.9–1.4 μm range, following Kirkpatrick et al. (2010). Both target and template spectra were normalized to their median flux, and reduced χ^2 values were computed to identify the best-matching templates. The assigned spectral type corresponds to the top match, while the uncertainty (± 0.5 or ± 1.0 subtype) reflects the separation between the best and second-best fits. Classifications were validated through visual inspection. We also tested an alternative method that removed linear slopes between spectra before comparison, which had no notable effect.

3. GRAVITY INDICATORS: METHODS AND ANALYSIS

Our study focuses on gravity-sensitive features within spectral types M5.5–L0, as shown in Figure 1 and Figure 2. Following the approach of AL13, we calculated gravity-sensitive indices for the full sample, with results presented in Table 2. The methodology, based on AL13, is detailed in Appendix B.

We also measured the equivalent widths (EWs) of the KI lines at 1.1692, 1.1778, and 1.2529 μm using the equivalent width function from the `Specutils` Python package (Astropy-Specutils Development Team 2019). Uncertainties on the EW measurements were estimated by scaling the mean flux uncertainty relative to the continuum level and propagating it across the line region, accounting for the number of spectral data points. Results are reported in Table A1.

Based on the index values in Table 2, we assigned gravity classifications using the VL-G (very low gravity), INT-G (intermediate gravity), and FLD-G (field gravity) categories defined in AL13, as illustrated in Figure 3 and Figure 4. Scores were assigned per index as follows: for FeH_J , FeH_Z , and KI_J , values below the VL-G threshold received a score of 2, between VL-G and INT-G a score of 1, and above INT-G a score of 0. For VO_z and $H\text{-cont}$, scoring was reversed. A combined FeH score was derived by evaluating both FeH_Z and FeH_J , taking the higher of the two.

Whereas AL13 used a “?” designation when an index score was intermediate but had a 1σ uncertainty overlapping with field gravity, we followed the approach of Aller et al. (2016) and Martin et al. (2017), opting not to use this label. Instead, we used a Monte Carlo approach to more robustly quantify uncertainty in the gravity classification. For each index, we generated 10,000 synthetic

values drawn from a Gaussian distribution defined by the measured mean and variance. From these realizations, we calculated a distribution of scores, and we report the mean and standard deviation to reflect both the central tendency and associated uncertainty.

The final gravity class was based on the median of the four main scores (FeH , VO_z , KI_J , $H\text{-cont}$): values ≤ 0.5 were classified as FLD-G, between 0.5–1.5 as INT-G, and ≥ 1.5 as VL-G. Table 2 presents the gravity scores and corresponding classifications for objects with spectral types. As in Gonzales et al. (2019), half spectral types were rounded to the nearest integer.

4. RESULTS AND DISCUSSION

4.1. Gravity Anomalies in Exoplanet-hosting M-Dwarfs

Gonzales et al. (2019) compared TRAPPIST-1’s AL13 gravity indices across multiple datasets, including SpeX and FIRE spectra, and found a mix of youth-like and field-age features. More recently, Davoudi et al. (2024) applied a similar methodology using JWST/NIRISS data and confirmed intermediate-gravity (INT-G) classifications across all indices. Specifically, TRAPPIST-1 falls within the INT-G regime gravity indices are plotted against spectral type, but aligns more so with field gravity (FLD-G) in equivalent width comparisons. Certain indices, such as $H\text{-cont}$ and KI_J , show field-like values in FIRE medium-resolution spectra. Together, these subtle but consistent deviations across datasets support an INT-G classification for TRAPPIST-1. This interesting combination of field-age characterizations and low-gravity spectral features has been interpreted as evidence for external influences such as magnetic activity or tidal interactions with orbiting planets (Gonzales et al. 2019).

A similar pattern is observed in Teegarden’s Star, an M7.5 dwarf classified as a β (intermediate-gravity) source by Gagné et al. (2015) based on SpeX/Prism spectra. Its gravity indices—including a low FeH_Z (1.0699 ± 0.0040), low KI_J (1.0511 ± 0.0065), and elevated $H\text{-cont}$ (0.9974 ± 0.0049)—deviate from typical field M7.5 dwarfs, further reinforcing the intermediate-gravity classification.

Our findings extend this trend to SPECULOOS-2, SPECULOOS-3, and LHS 3154. Each shows spectral signatures indicative of intermediate gravity, supporting the hypothesis that such anomalies may be linked to the presence of close-in planetary companions. SPECULOOS-2 hosts two planets with orbital periods of 2.73 days (SPECULOOS-2 b) and 8.46 days (SPECULOOS-2 c) (Delrez et al. 2022). SPECULOOS-3 hosts a single planet ultra-short-period planet (0.72 d; Gillon et al. 2024), and LHS 3154 hosts a planet with

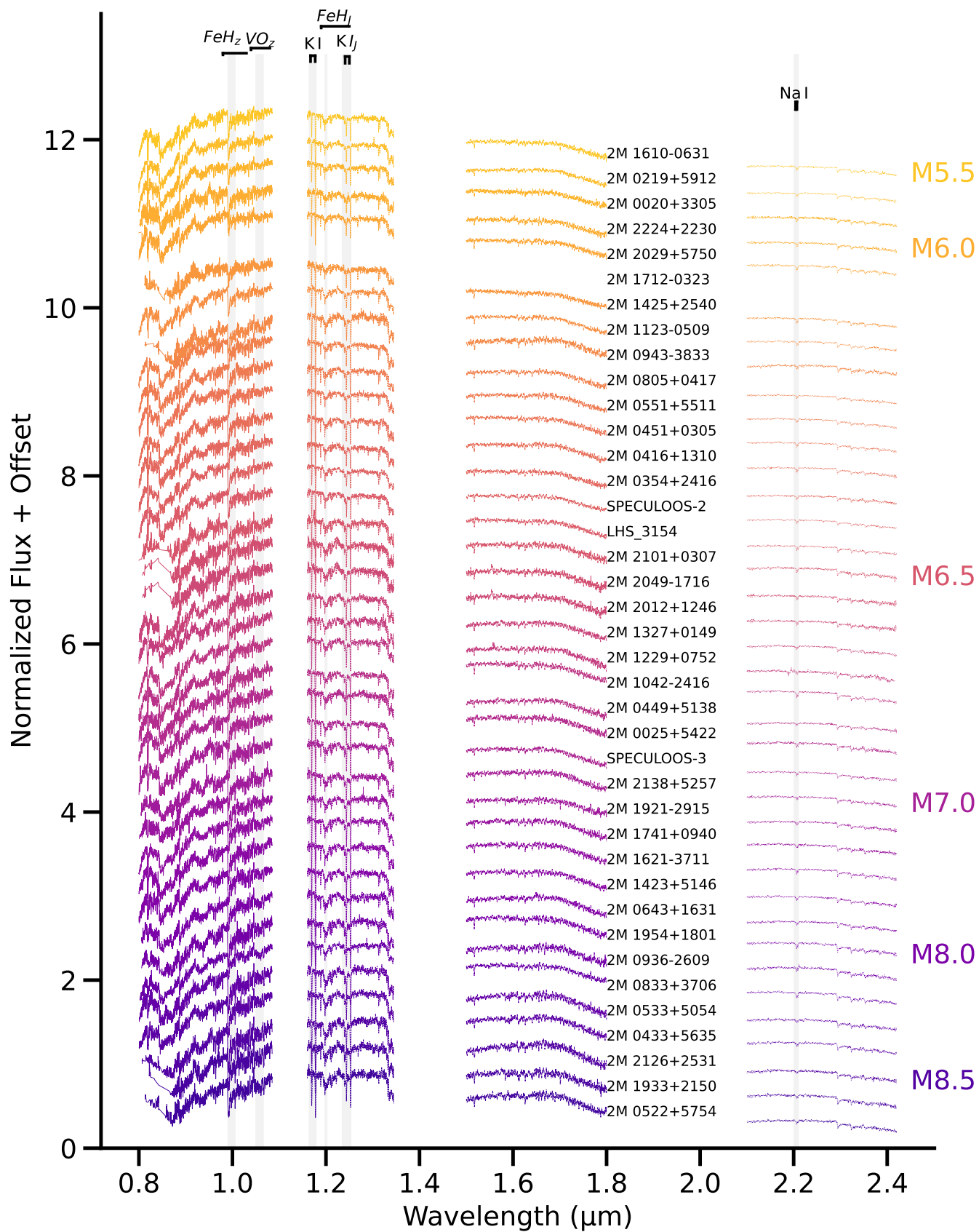


Figure 1. Near-IR SpeX/SXD spectra ($R \sim 2000$) of the M dwarfs in our sample. Spectral types and positions of significant gravity-sensitive features are indicated.

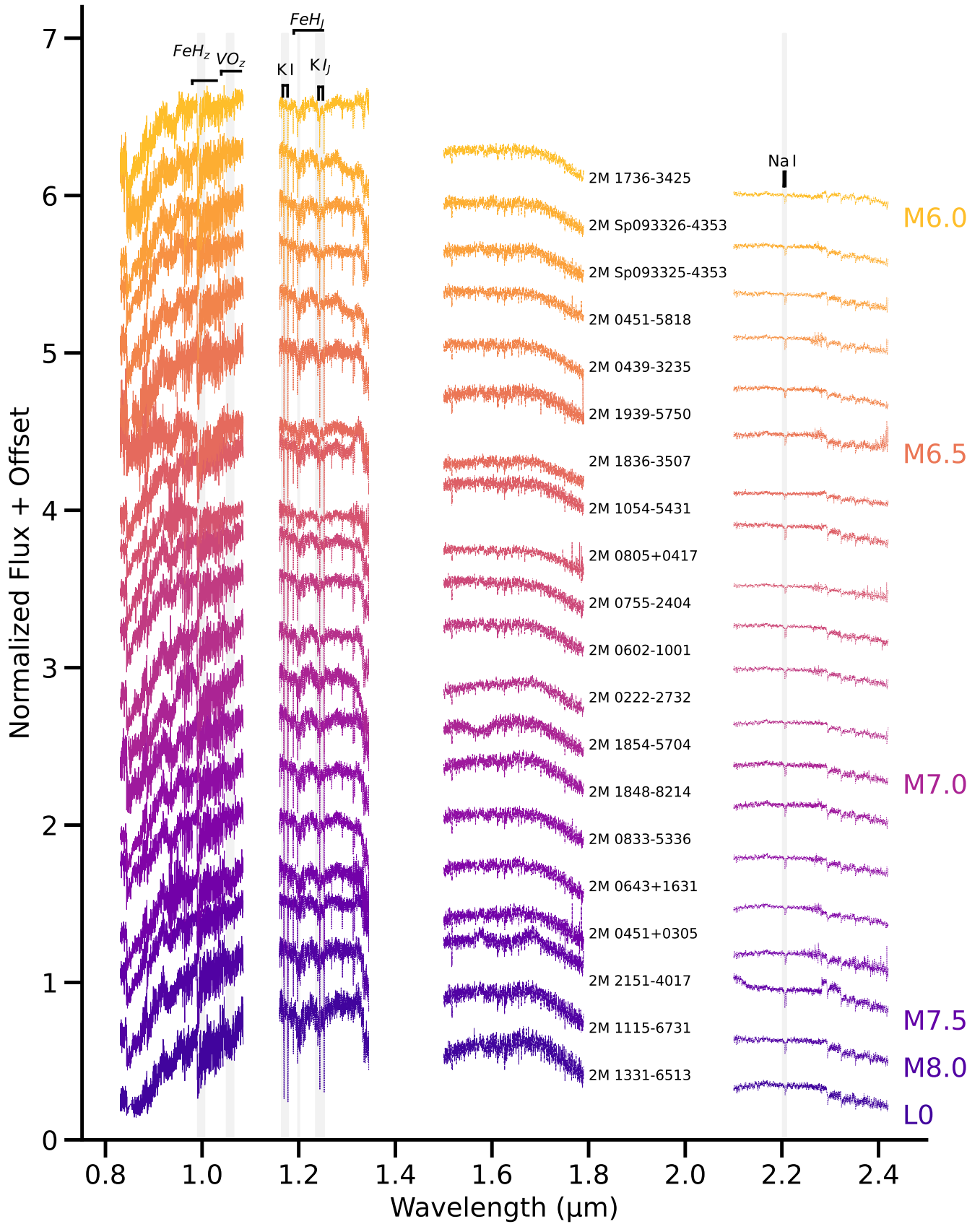


Figure 2. Near-IR FIRE spectra ($R \sim 8000$) of the M dwarfs in our sample. Spectral types and positions of significant gravity-sensitive features are indicated.

Table 2. Gravity Indices and Classifications

Object (2MASS J)	FeHz index	FeHJ index	VOz index	KIJ index	H-cont index	Gravity Score	Gravity Class
00202922+3305081	1.069 ± 0.014	1.050 ± 0.010	1.016 ± 0.012	1.046 ± 0.011	0.988 ± 0.009	0n01	FLD-G
00251602+5422547	1.149 ± 0.015	1.101 ± 0.009	0.998 ± 0.011	1.086 ± 0.011	0.983 ± 0.006	0n01	FLD-G
02195603+5919273	1.074 ± 0.011	1.050 ± 0.007	1.036 ± 0.009	1.053 ± 0.009	0.993 ± 0.008	0n01	FLD-G
02224767-2732349	1.157 ± 0.017	1.107 ± 0.009	1.053 ± 0.010	1.084 ± 0.011	0.980 ± 0.007	0n00	FLD-G
03544620+2416246	1.071 ± 0.026	1.058 ± 0.014	1.022 ± 0.022	1.055 ± 0.014	0.992 ± 0.008	0n01	FLD-G
04164276+1310587	1.132 ± 0.013	1.098 ± 0.008	1.013 ± 0.010	1.058 ± 0.010	0.984 ± 0.005	0n00	FLD-G
04333002+5635320	1.214 ± 0.016	1.132 ± 0.010	1.019 ± 0.012	1.081 ± 0.011	0.980 ± 0.007	0n01	FLD-G
04393407-3235516	1.094 ± 0.010	1.071 ± 0.005	1.010 ± 0.007	1.057 ± 0.008	0.982 ± 0.005	0n00	FLD-G
04490464+5138412	1.133 ± 0.014	1.112 ± 0.008	1.033 ± 0.011	1.072 ± 0.010	0.977 ± 0.009	0n00	FLD-G
04511406+0305285(FIRE)	1.169 ± 0.026	1.103 ± 0.014	1.047 ± 0.019	1.083 ± 0.016	0.981 ± 0.007	0n01	FLD-G
04511406+0305285(SpeX)	1.146 ± 0.013	1.121 ± 0.007	1.062 ± 0.009	1.081 ± 0.009	0.983 ± 0.006	1n01	INT-G
04513734-5818519	1.168 ± 0.011	1.096 ± 0.006	1.021 ± 0.007	1.077 ± 0.008	0.976 ± 0.004	0n00	FLD-G
05220976+5754046	1.243 ± 0.025	1.157 ± 0.012	1.052 ± 0.017	1.077 ± 0.014	0.975 ± 0.005	1n11	INT-G
05335379+5054170	1.281 ± 0.019	1.161 ± 0.011	1.009 ± 0.013	1.092 ± 0.012	0.961 ± 0.009	0n00	FLD-G
05512511+5511208	1.121 ± 0.013	1.094 ± 0.008	1.013 ± 0.011	1.064 ± 0.010	0.976 ± 0.007	0n00	FLD-G
06020172-1001565	1.127 ± 0.011	1.085 ± 0.006	1.007 ± 0.007	1.053 ± 0.008	0.982 ± 0.006	0n11	INT-G
06431389+1631428(FIRE)	1.212 ± 0.022	1.119 ± 0.012	1.009 ± 0.016	1.088 ± 0.014	0.980 ± 0.007	0n01	FLD-G
06431389+1631428(SpeX)	1.168 ± 0.011	1.111 ± 0.006	1.006 ± 0.007	1.070 ± 0.008	0.984 ± 0.005	0n00	FLD-G
07552745-2404374	1.091 ± 0.012	1.077 ± 0.006	1.036 ± 0.008	1.056 ± 0.009	0.980 ± 0.006	1n10	INT-G
08055713+0417035(FIRE)	1.139 ± 0.012	1.080 ± 0.007	0.994 ± 0.009	1.055 ± 0.009	0.979 ± 0.008	0n11	INT-G
08055713+0417035(SpeX)	1.130 ± 0.009	1.085 ± 0.005	1.009 ± 0.007	1.053 ± 0.007	0.981 ± 0.005	0n00	FLD-G
08330310+3706083	1.139 ± 0.015	1.108 ± 0.009	1.062 ± 0.012	1.072 ± 0.011	0.971 ± 0.009	1n11	INT-G
08334323-5336417	1.121 ± 0.011	1.093 ± 0.006	1.057 ± 0.008	1.069 ± 0.008	0.975 ± 0.005	0n00	FLD-G
09332510-4353384	1.138 ± 0.016	1.110 ± 0.008	0.998 ± 0.009	1.070 ± 0.011	0.972 ± 0.007	0n00	FLD-G
09332625-4353366	1.164 ± 0.015	1.114 ± 0.008	1.003 ± 0.009	1.062 ± 0.010	0.972 ± 0.007	0n00	FLD-G
09365564-2609422	1.282 ± 0.021	1.170 ± 0.011	1.029 ± 0.014	1.102 ± 0.012	0.967 ± 0.005	0n01	FLD-G
09432994-3833560	1.152 ± 0.013	1.083 ± 0.008	1.001 ± 0.010	1.064 ± 0.010	0.983 ± 0.006	0n00	FLD-G
10424135-2416050	1.150 ± 0.025	1.112 ± 0.020	1.036 ± 0.023	1.069 ± 0.022	0.970 ± 0.012	0n00	FLD-G
10542786-5431322	1.103 ± 0.017	1.086 ± 0.009	1.040 ± 0.011	1.068 ± 0.012	0.983 ± 0.008	1n01	INT-G
11155037-6731332	1.142 ± 0.015	1.115 ± 0.008	1.061 ± 0.010	1.085 ± 0.010	0.985 ± 0.006	1n20	INT-G
11231964-0509045	1.148 ± 0.015	1.086 ± 0.009	1.002 ± 0.011	1.063 ± 0.011	0.978 ± 0.010	0n00	FLD-G
12294530+0752379	1.154 ± 0.013	1.088 ± 0.008	0.998 ± 0.010	1.058 ± 0.010	0.979 ± 0.009	0n10	FLD-G
13273095+0149384	1.176 ± 0.016	1.107 ± 0.009	1.012 ± 0.012	1.071 ± 0.011	0.993 ± 0.010	0n02	INT-G
13313937-6513056	1.241 ± 0.024	1.198 ± 0.011	1.119 ± 0.008	1.119 ± 0.010	0.969 ± 0.008	1001	INT-G
14230252+5146303	1.204 ± 0.017	1.081 ± 0.011	1.009 ± 0.013	1.068 ± 0.013	0.996 ± 0.009	0n02	INT-G
14253465+2540050	1.122 ± 0.012	1.082 ± 0.008	1.013 ± 0.010	1.055 ± 0.010	0.981 ± 0.007	0n00	FLD-G
16105843-0631325	1.112 ± 0.013	1.078 ± 0.008	1.005 ± 0.010	1.061 ± 0.010	0.976 ± 0.009	0n00	FLD-G
16210447-3711373	1.191 ± 0.019	1.129 ± 0.011	1.032 ± 0.014	1.089 ± 0.012	0.979 ± 0.005	0n00	FLD-G
17120433-0323300	1.126 ± 0.012	1.092 ± 0.008	1.019 ± 0.010	1.068 ± 0.010	0.977 ± 0.008	0n00	FLD-G
17364180-3425459	1.082 ± 0.013	1.084 ± 0.007	1.019 ± 0.009	1.068 ± 0.009	0.982 ± 0.006	0n00	FLD-G
17415439+0940537	1.184 ± 0.015	1.111 ± 0.009	1.009 ± 0.012	1.075 ± 0.011	0.979 ± 0.006	0n00	FLD-G
18365842-3507176	1.279 ± 0.027	1.123 ± 0.011	0.977 ± 0.013	1.108 ± 0.013	0.966 ± 0.007	0n00	FLD-G
18485108-8214422	1.118 ± 0.016	1.097 ± 0.008	1.028 ± 0.010	1.082 ± 0.011	0.978 ± 0.007	0n00	FLD-G
18545092-5704417	1.281 ± 0.018	1.101 ± 0.008	1.018 ± 0.009	1.084 ± 0.010	0.984 ± 0.007	0n01	FLD-G
19212977-2915507	1.170 ± 0.012	1.118 ± 0.008	1.023 ± 0.010	1.072 ± 0.009	0.992 ± 0.008	0n02	INT-G
19332754+2150009	1.254 ± 0.026	1.159 ± 0.012	1.075 ± 0.018	1.104 ± 0.014	0.962 ± 0.012	1n01	INT-G
19395199-5750339	1.103 ± 0.025	1.099 ± 0.012	1.038 ± 0.014	1.076 ± 0.014	0.986 ± 0.009	1n01	INT-G
19544358+1801581	1.176 ± 0.016	1.136 ± 0.009	1.058 ± 0.012	1.078 ± 0.011	0.986 ± 0.009	0n02	INT-G
20125255+1246315	1.180 ± 0.019	1.101 ± 0.011	1.024 ± 0.015	1.075 ± 0.013	0.993 ± 0.012	0n02	INT-G
20291194+5750317	1.123 ± 0.015	1.080 ± 0.010	0.995 ± 0.012	1.061 ± 0.011	0.979 ± 0.009	0n00	FLD-G
20495272-1716083	1.147 ± 0.022	1.096 ± 0.013	1.001 ± 0.017	1.074 ± 0.015	0.978 ± 0.007	0n00	FLD-G
21010483+0307047	1.140 ± 0.022	1.097 ± 0.013	1.003 ± 0.017	1.075 ± 0.015	0.980 ± 0.014	0n00	FLD-G
21265788+2531080	1.277 ± 0.024	1.163 ± 0.013	1.039 ± 0.017	1.104 ± 0.014	0.972 ± 0.010	0n01	FLD-G
21381698+5257188	1.198 ± 0.016	1.139 ± 0.010	1.008 ± 0.012	1.076 ± 0.011	0.987 ± 0.006	0n01	FLD-G
21513137-4017229	1.097 ± 0.013	1.067 ± 0.007	1.026 ± 0.009	1.076 ± 0.010	0.984 ± 0.005	2n11	INT-G
22244238+2230425	1.146 ± 0.021	1.067 ± 0.013	0.997 ± 0.016	1.065 ± 0.014	0.994 ± 0.013	0n01	FLD-G
SPECULOOS-2	1.056 ± 0.010	1.039 ± 0.007	1.009 ± 0.008	1.039 ± 0.009	0.985 ± 0.007	2n10	INT-G
SPECULOOS-3	1.139 ± 0.018	1.070 ± 0.011	1.011 ± 0.014	1.056 ± 0.013	0.993 ± 0.012	1n12	INT-G
LHS 3154	1.061 ± 0.016	1.056 ± 0.010	1.023 ± 0.013	1.054 ± 0.012	0.997 ± 0.010	1n02	INT-G
TRAPPIST-1(FIRE)	1.105 ± 0.001	1.110 ± 0.009	1.084 ± 0.001	1.062 ± 0.001	0.951 ± 0.001	1n10	INT-G
TRAPPIST-1(SpeX)	1.119 ± 0.001	1.093 ± 0.010	1.070 ± 0.002	1.070 ± 0.001	0.971 ± 0.001	1n01	INT-G

NOTE—For TRAPPIST-1, we used the medium-resolution SpeX/SXD and FIRE spectra results derived by [Gonzales et al. \(2019\)](#).

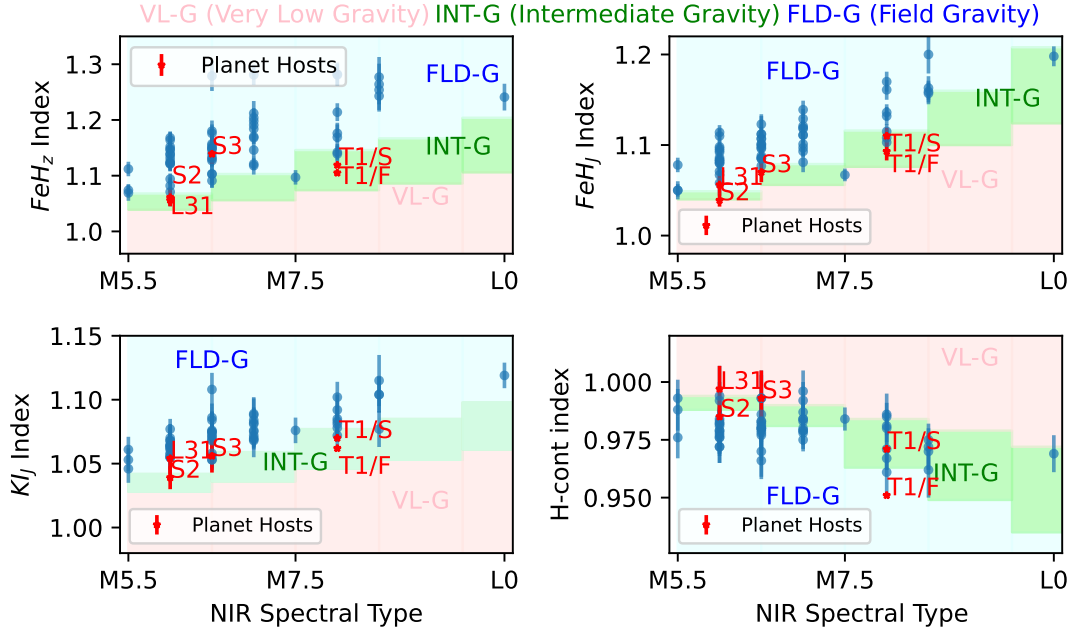


Figure 3. Gravity indices (FeH_z , FeH_J , K_{J1} and $H\text{-cont}$) vs. NIR spectral type for M dwarfs in our sample. The color-coded regions represent different gravity classifications: Very Low Gravity (VL-G, light pink), Intermediate Gravity (INT-G, light green), and Field Gravity (FLD-G, light blue). SPECULOOS-2 (S2), SPECULOOS-3 (S3), LHS 3154 (L31) and the FIRE and SpeX spectra measurements of TRAPPIST-1 (T1/F and T1/S) are highlighted as red stars.

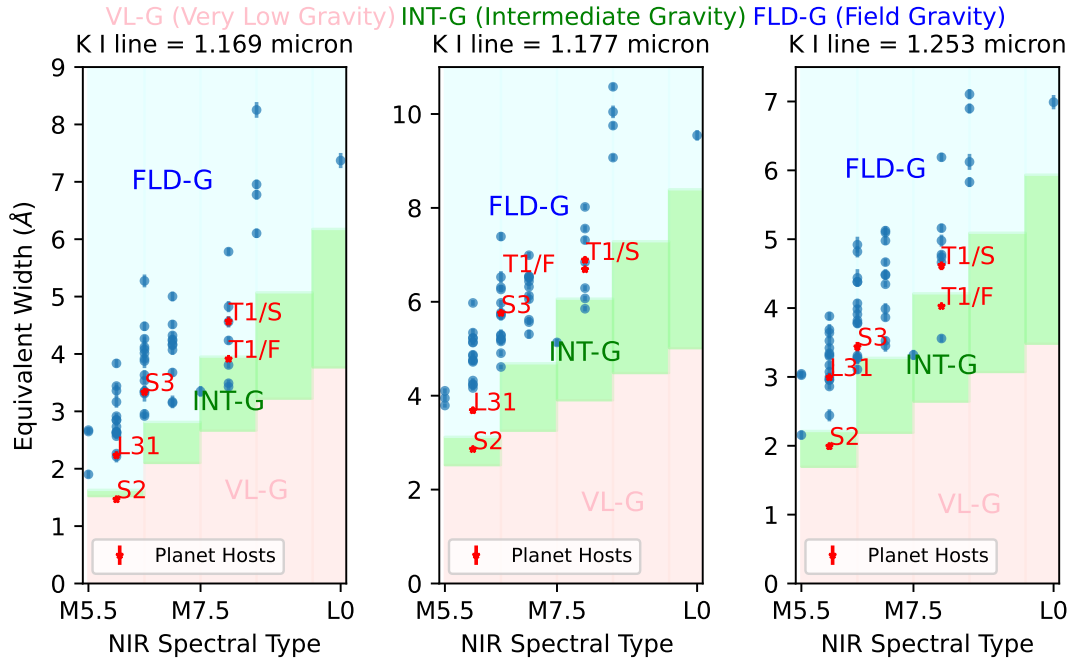


Figure 4. EWs for the K I lines in the J band vs. NIR spectral type for M dwarfs in our sample. The figure elements are the same as in Figure 3. The panels display: (a) NIR spectral type vs. K I $1.169\ \mu\text{m}$ EW, (b) NIR spectral type vs. K I $1.177\ \mu\text{m}$ EW, and (c) NIR spectral type vs. K I $1.253\ \mu\text{m}$ EW.

an orbital period of 3.72 days (Stefánsson et al. 2023). Relevant spectral indices for these systems are presented in Figure 3 and Figure 4.

4.2. *Assessing the Relationship between Surface Gravity and Planet Occurrence*

In this section, we evaluate whether surface gravity—quantified via overall classification or specific spectral features—shows a statistical relationship with the presence of close-in exoplanets in our sample.

4.3. *Gravity Classification and Planet Occurrence*

We investigated the relationship between spectroscopic gravity classification and exoplanet-hosting status among our sample of late-M dwarfs. As an initial test, we applied Fisher’s exact test (Fisher 1922) under the null hypothesis that gravity class is independent of planet-hosting status. The test returned a p -value of 0.0116, corresponding to a 2.27σ result, suggesting a marginally significant association.

However, our sample is not volume-complete and exhibits biases in the target selection, particularly for TRAPPIST-1, SPECULOOS-2, and LHS 3154, for which spectra were obtained only after planetary signals had been identified. To mitigate the effects of this selection bias and sample incompleteness, we performed a regularized logistic regression using gravity class as a predictor for planet-hosting status, weighted by the inverse cube of Gaia distances (Gaia Collaboration et al. 2023) to approximate a volume-limited correction. We employed ridge (L2) regularization (Hoerl & Kennard 1970; Pedregosa et al. 2011) to stabilize the fit in the presence of small-sample effects and potential quasi-separation.

The logistic regression results revealed no statistically significant increase in the likelihood of hosting a close-in planet for intermediate-gravity (INT-G) stars compared to field-gravity (FLD-G) stars. This finding suggests that the apparent signal in the unweighted Fisher’s test may be influenced by the selection effects in the sample. Thus, while the marginally significant result from the Fisher’s exact test is tantalizing, a more definitive assessment of the connection between gravity classification and exoplanet occurrence will require a volume-limited, unbiased spectroscopic survey of ultracool dwarfs.

In the following, we explore further whether any of the spectral indices related to the gravity classification show a unique relationship to known planet occurrence in our sample.

4.4. *Spectral Index Behavior and Planet Occurrence*

To statistically assess whether gravity-sensitive features differ between stars with and without *detected*

planets, we performed Kolmogorov–Smirnov (KS) tests (Kolmogorov 1933; Smirnov 1948) on each gravity index from Table 2. The results are summarized in ???. We caution, however, that the sample includes a known selection bias: spectra for three of the known exoplanet host stars were obtained *after* their exoplanets had been detected. This targeted follow-up may skew the apparent differences between planet-hosting and non-hosting stars, complicating interpretation of any planet occurrence trends.

Figure 5 presents empirical cumulative distribution function (ECDF) comparisons for eight gravity indices, comparing stars with and without detected transiting planets. However, we caution that stars classified as “without planets” may still host undetected planets, such as non-transiting systems or planets below the detection threshold. Therefore, the distinction between planet-hosting and non-hosting stars is not absolute, and any observed differences should be interpreted with care.

In each panel, the KS statistic (D) represents the maximum vertical distance between the two ECDFs, providing a quantitative measure of the discrepancy between the distributions. Among the indices tested, only FeH_z exhibited a marginal difference between the two populations (KS statistic $D = 0.604$, $p = 0.043$), reaching the 2σ significance threshold. This may suggest a potential shift in its distribution associated with planet presence, though the result remained statistically tentative. All other indices, including FeH_J , VO_z , KI_J , and iron abundance $[\text{Fe}/\text{H}]$, showed no statistically significant differences ($p > 0.05$).

To further investigate whether stars hosting detected transiting exoplanets differ in their gravity-sensitive features, we performed a chi-squared test on each gravity index. The tests compared values from two groups, stars with detected exoplanets and stars without. For FeH_z , the test yielded $\chi^2 = 9.342$ with a p -value of 0.052, suggesting a marginally significant association with planet presence, though it does not reach the standard threshold for significance ($p < 0.05$). No such trend was observed for the other indices, with χ^2 values ranging from 34.7 to 65.0 and corresponding p -values between 0.118 and 0.604.

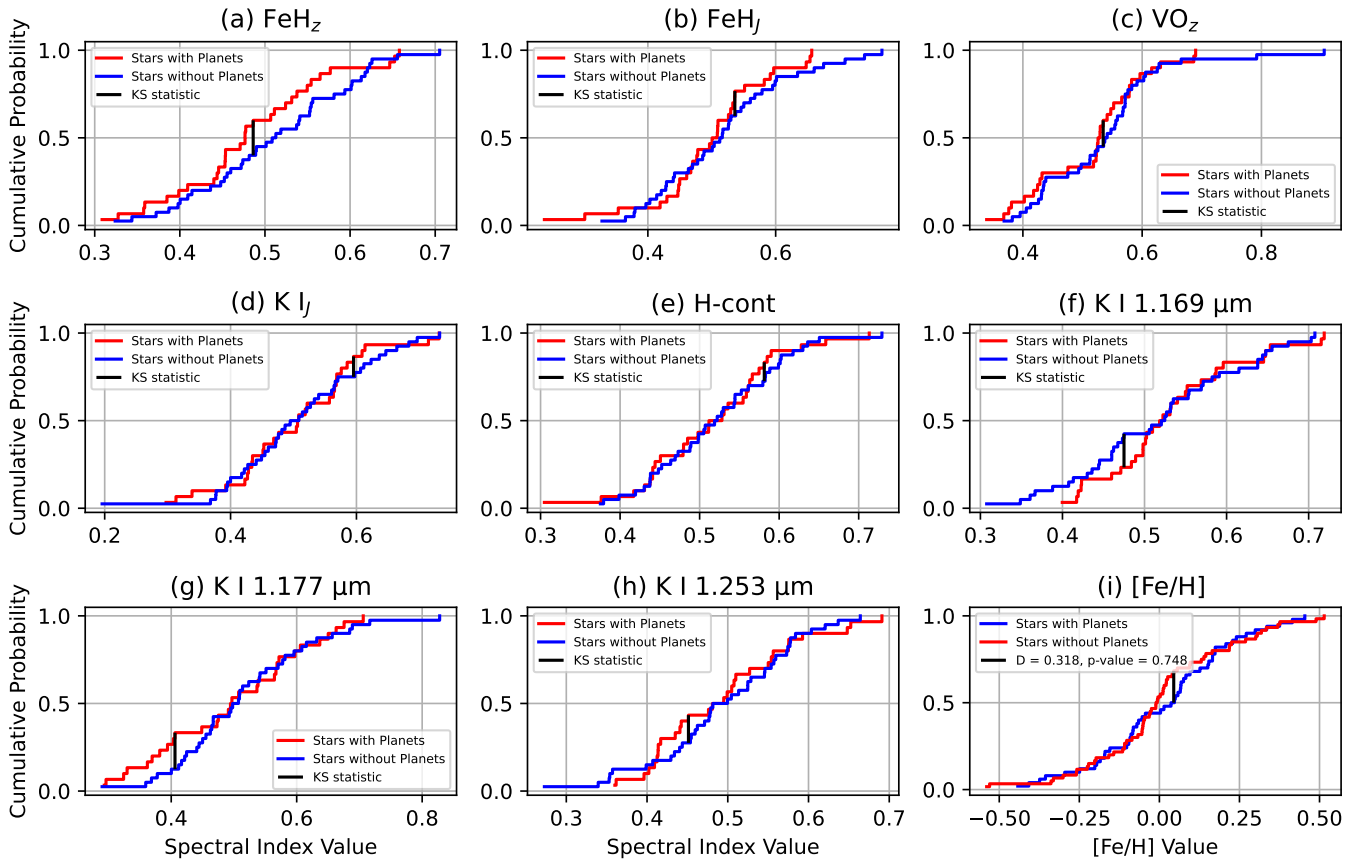
4.5. *Interplay Between Gravity and Metallicity Indicators in Late M-dwarf Spectra*

4.5.1. *Metallicity Estimation and Relationship to Planet Occurrence*

To explore potential trends between planet occurrence and metallicity ($[\text{Fe}/\text{H}]$), we calculated $[\text{Fe}/\text{H}]$ values for

Table 3. Statistical correlations between gravity indices and metallicity, with test statistic, p -value, and Gaussian equivalent σ . Results with $\sigma > 3$ are bolded.

Gravity Index	KS test with planet presence			Pearson Correlation with [Fe/H]			Spearman Correlation with [Fe/H]		
	D	p	σ	r	p	σ	r_s	p	σ
FeH _z	0.604	0.043	2.02	-0.277	0.031	2.15	-0.458	0.001	3.29
FeH _J	0.511	0.129	1.52	-0.138	0.289	1.06	-0.229	0.075	1.78
VO _z	0.364	0.471	0.72	0.288	0.025	2.24	0.348	0.006	2.74
K I _J	0.550	0.083	1.73	-0.214	0.097	1.66	-0.245	0.057	1.90
H-cont	0.386	0.402	0.83	0.160	0.217	1.23	0.187	0.149	1.44
K I 1.169 μm	0.364	0.471	0.72	-0.133	0.305	1.03	-0.231	0.073	1.79
K I 1.177 μm	0.400	0.353	0.93	-0.170	0.191	1.30	-0.268	0.051	1.96
K I 1.253 μm	0.311	0.671	0.42	-0.195	0.132	1.51	-0.322	0.011	2.54

**Figure 5.** ECDF plots for eight gravity indices, comparing stars with and without detected planets using the Kolmogorov–Smirnov (KS) test. Each panel shows the empirical cumulative distribution functions (ECDFs) for the two samples, with the KS statistic (D) indicated by a solid vertical line representing the maximum vertical difference between the distributions. Panel (a) shows FeH_z, where a significant difference is observed between the two groups, as indicated by the larger KS statistic. For all other indices, including FeH_J, VO_z, K I_J, and metallicity, the distributions do not show significant differences ($p > 0.05$). The x-axis represents the spectral index values, and the y-axis represents the cumulative probability.

all stars in our sample using the `splat` Python package²

(Schneider et al. 2016a; Burgasser & Splat Development Team 2017a). For mid- and late-type M dwarfs, we estimated metallicities using the EWs of the Na I (2.205 μm) and Ca I (2.263 μm) absorption features, in combination

² <https://gist.github.com/brackham/26b305919252f9bdabd2b56d463934d3>

with the H₂O–K2 index and the calibration provided by Mann et al. (2014), following the method of Rojas-Ayala et al. (2010, 2012). EWs were measured using the `Specutils` Python package, with uncertainties estimated via Monte Carlo simulations based on flux uncertainties (see Delrez et al. 2022). A systematic uncertainty of 0.07 dex from the Mann et al. (2014) calibration was added in quadrature to the measurement errors.

Our analysis revealed no significant correlation between [Fe/H] and planet occurrence within our sample, as indicated by the KS test (KS statistic = 0.318, p-value = 0.748; see panel (i) of Figure 5).

4.5.2. Metallicity Dependence of Gravity-sensitive Indices

Beyond planet occurrence, we also investigated whether gravity-sensitive spectral indices exhibit systematic trends with stellar metallicity. To do so, we calculated both Pearson and Spearman correlation coefficients between [Fe/H] and a set of gravity-sensitive spectral indices (see ??). While Pearson’s test identifies strictly linear relationships, Spearman’s rank-based test is sensitive to broader monotonic trends, including non-linear or saturating behaviors.

Among the indices tested, FeH_z and VO_z showed the strongest correlations with metallicity. However, only the Spearman test result for FeH_z exceeded the 3 σ threshold, indicating a robust inverse relationship between FeH_z and [Fe/H]. This result reinforces the finding that FeH_z is sensitive to metallicity in addition to gravity. VO_z also showed moderate positive correlations with metallicity in both Pearson and Spearman tests, although only at the 2 σ level. Similarly, the K I 1.253 μ m feature shows a weak anti-correlation with [Fe/H], though only at the 2 σ level for the Spearman test.

Overall, the tendency for stronger correlations in the Spearman tests suggests that metallicity influences gravity-sensitive features in complex, non-linear ways, underscoring the need to consider both composition and gravity when interpreting M-dwarf spectra.

4.5.3. Interpreting the FeH_z–[Fe/H] Anti-Correlation

The strongest correlation we observe is an inverse relationship between FeH_z and [Fe/H], which merits further interpretation given its potential implications for both spectral diagnostics and stellar characterization. At face value, the negative correlation between FeH_z and [Fe/H] is somewhat unexpected, as the FeH_z index traces the strength of the FeH molecular feature, which is generally assumed to increase with iron abundance. However, the FeH_z index is sensitive to both surface gravity and metallicity: lower gravity weakens FeH absorption, potentially offsetting the impact of metallicity.

This dual sensitivity offers a plausible explanation for the observed anti-correlation, particularly if metal-rich stars tend to have low gravities due to either enhanced opacities throughout the photosphere or relative youth.

To test whether metallicity alone could explain differences in gravity classifications, we performed a Kruskal–Wallis H test (Kruskal & Wallis 1952) comparing [Fe/H] across gravity classes in our sample. The result was not statistically significant ($H = 1.99$, $p = 0.16$), indicating no strong evidence that [Fe/H] differs between FLD-G and INT-G objects in our sample. This suggests that the relationship between surface gravity and metallicity in our sample is not straightforward, and thus the observed FeH_z–[Fe/H] anti-correlation may reflect the influence of other factors such as chemical abundances. This reasoning is in line with the findings of Gonzales et al. (2019), who found no evidence for low metallicity mimicking low-gravity spectral features for TRAPPIST-1.

Another possible explanation for the FeH_z–[Fe/H] anti-correlation is that stellar activity may also modulate FeH absorption. In such cases, FeH_z may not be a pure gravity indicator, but could reflect a combination of metallicity and activity-driven effects. For example, while low metallicity might intrinsically weaken FeH absorption, elevated activity levels, by contrast, could enhance it. This interplay could produce an inverse correlation between FeH_z and [Fe/H], complicating efforts to disentangle gravity, metallicity, and activity influences on the spectral features.

5. CONCLUSIONS

We present a comprehensive analysis of gravity-sensitive spectral indices in 57 ultracool M dwarfs, ranging from M5.5 to L0, including the exoplanet-hosting stars TRAPPIST-1, SPECULOOS-2, SPECULOOS-3, and LHS 3154. Our study investigates the relationship between spectral gravity indices and exoplanet presence in late-M dwarfs. The main findings are as follows.

1. We find that exoplanet-hosting M dwarfs, such as SPECULOOS-2, SPECULOOS-3, and LHS 3154, exhibit unusual spectral features similar to those of TRAPPIST-1 and Teegarden’s Star. These peculiarities suggest an intermediate-gravity classification, which is unexpected for field-age stars. This finding raises the possibility that factors beyond stellar age may influence the gravity-sensitive spectral features observed in exoplanet-hosting M dwarfs.

One possible explanation we explore is that increased metallicity could inflate stellar radii by

enhancing atmospheric opacity, thereby mimicking low-gravity signatures in spectral indices. At the same time, higher metallicity could reasonably influence planet formation efficiency. However, the connection between anomalous gravity indices and planet occurrence is not yet well constrained by current observations. Nonetheless, this possible relationship underscores the need for caution when using spectral diagnostics to infer age and gravity in exoplanet-hosting ultracool dwarfs.

2. We examined whether the presence of exoplanets correlates with specific gravity-sensitive spectral features, as tidal interactions or magnetic activity may modify these indices in exoplanet-hosting M dwarfs. Both KS and χ^2 tests identified FeH_z as the most promising index linked to planet presence. The KS test yielded $D = 0.604$ with $p = 0.043$, while the χ^2 test returned $\chi^2 = 9.342$ and $p = 0.052$ —both suggesting a possible trend near the 2σ level. The close agreement between these p -values reinforces the potential relevance of FeH_z , though these marginal results are insufficient to support a definitive correlation. Other gravity indices showed no significant differences between stars with and without detected planets.
3. We also tested for a broader association between gravity class and planet occurrence. A Fisher’s exact test yielded a marginal 2.3σ association between intermediate-gravity classification and planet-hosting status. However, this signal was not recovered in a volume-weighted logistic regression, indicating that it may be driven by selection biases in the sample.
4. We observed strong correlations between metallicity and certain gravity-sensitive indices, particularly FeH_z and VO_z . FeH_z shows a robust inverse relationship with $[\text{Fe}/\text{H}]$ (Spearman $r_s = -0.458$, $p = 0.001$, 3.3σ), suggesting it is not solely a gravity indicator but is also sensitive to metallicity and potentially stellar activity. A Kruskal–Wallis H test revealed no significant difference in $[\text{Fe}/\text{H}]$ between FLD-G and INT-G objects ($H = 1.99$, $p = 0.16$), implying that the FeH_z – $[\text{Fe}/\text{H}]$ anti-correlation is not simply due to systematic metallicity differences across gravity classes. This

underscores the complex interplay between gravity, composition, and activity in shaping M-dwarf spectral features.

Given these findings, further research is needed to disentangle the effects of stellar activity, tidal interactions, and metallicity on the spectra of exoplanet-hosting stars. Stars with very short-period planets, such as SPECULOOS-3, may provide valuable insights into how close planetary orbits influence stellar spectra, especially in the context of magnetic interactions and activity levels.

ACKNOWLEDGMENTS

F. D. and M. G. acknowledge funding from the Belgian Federal Science Policy Office (BELSPO) for the BRAIN 2.0 project PORTAL (B2/212/P1/PORTAL). They thank the European Space Agency (ESA) and BELSPO for their support in the framework of the PRODEX Programme. M. G. is FNRS-F.R.S. Research Director. B.V.R. thanks the Heising-Simons Foundation for support. J.d.W. and B.V.R. acknowledge support from the European Research Council (ERC) Synergy Grant under the European Union’s Horizon 2020 research and innovation program (grant No. 101118581 — project REVEAL). This material is based upon work supported by the National Aeronautics and Space Administration under Agreement No. 80NSSC21K0593 for the program “Alien Earths”. The results reported herein benefited from collaborations and/or information exchange within NASA’s Nexus for Exoplanet System Science (NExSS) research coordination network sponsored by NASA’s Science Mission Directorate. Visiting Astronomer at the Infrared Telescope Facility, which is operated by the University of Hawaii under contract 80HQTR24DA010 with the National Aeronautics and Space Administration. This paper includes data gathered with the 6.5 meter Magellan Telescopes located at Las Campanas Observatory, Chile.

Software: SPLAT (Schneider et al. 2016b; Burgasser & Splat Development Team 2017b), Specutils (Astropy-Specutils Development Team 2019) NumPy (Harris et al. 2020), Matplotlib (Hunter 2007), Astropy (Astropy Collaboration et al. 2022), emcee (Foreman-Mackey et al. 2013), SciPy (Virtanen 2020)

APPENDIX

A. EQUIVALENT WIDTHS AND METALLICITY MEASUREMENTS

Table A1 presents the EW of the K I lines at 1.169 μm , 1.177 μm , and 1.253 μm , along with the metallicity ([Fe/H]) for each object in our sample.

$$\text{Index} = \frac{(\lambda_{\text{cont}2} - \lambda_{\text{line}})F_{\text{cont}1} + (\lambda_{\text{line}} - \lambda_{\text{cont}1})F_{\text{cont}2}}{(\lambda_{\text{cont}2} - \lambda_{\text{cont}1})F_{\text{line}}} \quad (\text{B1})$$

Here, λ refers to the central wavelengths of the continuum and line regions, and F is the average flux in each band. Band definitions are adopted from Table 4 of AL13, with one exception: for the H-cont index, we used a revised blue continuum window at 1.270 μm due to spectral coverage limits, ensuring consistency with the original index's sensitivity.

Index values are converted into discrete gravity scores (0–2) using spectral-type-dependent thresholds from Table 9 of AL13. For instance, an M7 object scores 2 for FeH_z if $\text{FeH}_z \leq 1.056$.

B. MEASURING SURFACE GRAVITY INDICATORS

We adopt the spectral index method developed by AL13, which uses a three-bandpass formula to quantify gravity-sensitive absorption features:

REFERENCES

- Aganze, C., Burgasser, A. J., Faherty, J. K., et al. 2016, *AJ*, 151, 46, doi: [10.3847/0004-6256/151/2/46](https://doi.org/10.3847/0004-6256/151/2/46)
- Aller, K. M., Liu, M. C., Magnier, E. A., et al. 2016, *ApJ*, 821, 120, doi: [10.3847/0004-637X/821/2/120](https://doi.org/10.3847/0004-637X/821/2/120)
- Allers, K. N., & Liu, M. C. 2013, *ApJ*, 772, 79, doi: [10.1088/0004-637X/772/2/79](https://doi.org/10.1088/0004-637X/772/2/79)
- Allers, K. N., Jaffe, D. T., Luhman, K. L., et al. 2007, *ApJ*, 657, 511, doi: [10.1086/510845](https://doi.org/10.1086/510845)
- Astropy Collaboration, Price-Whelan, A. M., Lim, P. L., et al. 2022, *ApJ*, 935, 167, doi: [10.3847/1538-4357/ac7c74](https://doi.org/10.3847/1538-4357/ac7c74)
- Astropy-Specutils Development Team. 2019, *Specutils: Spectroscopic analysis and reduction*, *Astrophysics Source Code Library*, record ascl:1902.012
- Bardalez Gagliuffi, D. C., Burgasser, A. J., Schmidt, S. J., et al. 2019, *ApJ*, 883, 205, doi: [10.3847/1538-4357/ab253d](https://doi.org/10.3847/1538-4357/ab253d)
- Burgasser, A. J., & Mamajek, E. E. 2017, *ApJ*, 845, 110, doi: [10.3847/1538-4357/aa7fea](https://doi.org/10.3847/1538-4357/aa7fea)
- Burgasser, A. J., & Splat Development Team. 2017a, in *Astronomical Society of India Conference Series*, Vol. 14, *Astronomical Society of India Conference Series*, 7–12, doi: [10.48550/arXiv.1707.00062](https://doi.org/10.48550/arXiv.1707.00062)
- Burgasser, A. J., & Splat Development Team. 2017b, in *Astronomical Society of India Conference Series*, Vol. 14, *Astronomical Society of India Conference Series*, 7–12, doi: [10.48550/arXiv.1707.00062](https://doi.org/10.48550/arXiv.1707.00062)
- Cruz, K. L., Kirkpatrick, J. D., & Burgasser, A. J. 2009, *AJ*, 137, 3345, doi: [10.1088/0004-6256/137/2/3345](https://doi.org/10.1088/0004-6256/137/2/3345)
- Cushing, M. C., Rayner, J. T., & Vacca, W. D. 2005, *ApJ*, 623, 1115, doi: [10.1086/428040](https://doi.org/10.1086/428040)
- Cushing, M. C., Vacca, W. D., & Rayner, J. T. 2004, *PASP*, 116, 362, doi: [10.1086/382907](https://doi.org/10.1086/382907)
- Davoudi, F., Rackham, B. V., Gillon, M., et al. 2024, *ApJL*, 970, L4, doi: [10.3847/2041-8213/ad5c6c](https://doi.org/10.3847/2041-8213/ad5c6c)
- Delrez, L., Murray, C. A., Pozuelos, F. J., et al. 2022, *A&A*, 667, A59, doi: [10.1051/0004-6361/202244041](https://doi.org/10.1051/0004-6361/202244041)
- Dreizler, S., Luque, R., Ribas, I., et al. 2024, *A&A*, 684, A117, doi: [10.1051/0004-6361/202348033](https://doi.org/10.1051/0004-6361/202348033)
- Filippazzo, J. C., Rice, E. L., Faherty, J., et al. 2015, *ApJ*, 810, 158, doi: [10.1088/0004-637X/810/2/158](https://doi.org/10.1088/0004-637X/810/2/158)
- Fisher, R. A. 1922, *Journal of the Royal Statistical Society*, 85, 87, doi: [10.2307/2340521](https://doi.org/10.2307/2340521)
- Foreman-Mackey, D., Hogg, D. W., Lang, D., & Goodman, J. 2013, *PASP*, 125, 306, doi: [10.1086/670067](https://doi.org/10.1086/670067)
- Gagné, J., Faherty, J. K., Cruz, K. L., et al. 2015, *ApJS*, 219, 33, doi: [10.1088/0067-0049/219/2/33](https://doi.org/10.1088/0067-0049/219/2/33)
- Gagné, J., Mamajek, E. E., Malo, L., et al. 2018, *ApJ*, 856, 23, doi: [10.3847/1538-4357/aaae09](https://doi.org/10.3847/1538-4357/aaae09)
- Gaia Collaboration, Vallenari, A., Brown, A. G. A., et al. 2023, *A&A*, 674, A1, doi: [10.1051/0004-6361/202243940](https://doi.org/10.1051/0004-6361/202243940)
- Gillon, M., Jehin, E., Lederer, S. M., et al. 2016, *Nature*, 533, 221, doi: [10.1038/nature17448](https://doi.org/10.1038/nature17448)
- Gillon, M., Triaud, A. H. M. J., Demory, B.-O., et al. 2017, *Nature*, 542, 456, doi: [10.1038/nature21360](https://doi.org/10.1038/nature21360)
- Gillon, M., Pedersen, P. P., Rackham, B. V., et al. 2024, *Nature Astronomy*, 8, 865, doi: [10.1038/s41550-024-02271-2](https://doi.org/10.1038/s41550-024-02271-2)

Table A1. Equivalent widths and metallicity calculated from our sample spectra.

Object	Spectrum	EW(K _I 1.169 μ m)	EW(K _I 1.177 μ m)	EW(K _I 1.253 μ m)	[Fe/H]
2MASS J00202922+3305081	SpeX	1.902 \pm 0.069	3.949 \pm 0.066	2.156 \pm 0.065	0.027 \pm 0.114
2MASS J00251602+5422547	SpeX	4.265 \pm 0.062	6.263 \pm 0.061	4.380 \pm 0.055	-0.188 \pm 0.096
2MASS J02195603+5919273	SpeX	2.673 \pm 0.047	3.791 \pm 0.045	3.045 \pm 0.043	0.100 \pm 0.084
2MASS J02224767-2732349	FIRE	5.273 \pm 0.112	7.390 \pm 0.092	4.819 \pm 0.084	-0.156 \pm 0.077
2MASS J03544620+2416246	SpeX	2.211 \pm 0.101	4.232 \pm 0.101	2.442 \pm 0.088	0.365 \pm 0.103
2MASS J04164276+1310587	SpeX	2.263 \pm 0.052	4.852 \pm 0.049	3.343 \pm 0.046	0.219 \pm 0.087
2MASS J04333002+5635320	SpeX	3.490 \pm 0.063	6.292 \pm 0.061	4.740 \pm 0.057	-0.139 \pm 0.102
2MASS J04393407-3235516	FIRE	2.610 \pm 0.067	4.164 \pm 0.056	2.963 \pm 0.052	-0.005 \pm 0.073
2MASS J04490464+5138412	SpeX	3.916 \pm 0.055	5.732 \pm 0.051	3.775 \pm 0.052	0.355 \pm 0.093
2MASS J04511406+0305285	SpeX	4.561 \pm 0.100	6.846 \pm 0.096	4.979 \pm 0.087	-0.109 \pm 0.121
2MASS J04511406+0305285	FIRE	5.002 \pm 0.084	6.992 \pm 0.069	5.124 \pm 0.065	0.084 \pm 0.075
2MASS J04513734-5818519	FIRE	3.836 \pm 0.073	5.976 \pm 0.060	3.882 \pm 0.057	-0.006 \pm 0.073
2MASS J05220976+5754046	SpeX	6.103 \pm 0.082	9.071 \pm 0.077	5.829 \pm 0.072	0.020 \pm 0.100
2MASS J05335379+5054170	SpeX	5.783 \pm 0.069	8.021 \pm 0.067	6.190 \pm 0.063	-0.230 \pm 0.107
2MASS J05512511+5511208	SpeX	2.916 \pm 0.057	5.131 \pm 0.053	3.420 \pm 0.052	0.213 \pm 0.092
2MASS J06020172-1001565	FIRE	2.956 \pm 0.077	4.906 \pm 0.064	3.108 \pm 0.061	-0.005 \pm 0.074
2MASS J06431389+1631428	SpeX	4.071 \pm 0.087	6.547 \pm 0.083	4.488 \pm 0.076	-0.107 \pm 0.116
2MASS J06431389+1631428	FIRE	4.323 \pm 0.068	6.437 \pm 0.056	4.667 \pm 0.053	-0.146 \pm 0.074
2MASS J07552745-2404374	FIRE	3.632 \pm 0.084	5.296 \pm 0.070	3.785 \pm 0.066	0.271 \pm 0.074
2MASS J08055713+0417035	SpeX	2.644 \pm 0.049	4.746 \pm 0.047	2.861 \pm 0.045	0.145 \pm 0.087
2MASS J08055713+0417035	FIRE	2.918 \pm 0.057	4.612 \pm 0.048	3.309 \pm 0.045	0.100 \pm 0.072
2MASS J08330310+3706083	SpeX	3.429 \pm 0.060	5.852 \pm 0.057	3.558 \pm 0.056	0.441 \pm 0.096
2MASS J08334323-5336417	FIRE	3.677 \pm 0.073	5.567 \pm 0.061	3.865 \pm 0.057	0.045 \pm 0.073
2MASS J09332510-4353384	FIRE	3.165 \pm 0.102	5.231 \pm 0.085	3.640 \pm 0.081	-0.093 \pm 0.077
2MASS J09332625-4353366	FIRE	3.360 \pm 0.102	5.343 \pm 0.084	3.686 \pm 0.081	-0.083 \pm 0.076
2MASS J09365564-2609422	SpeX	4.236 \pm 0.071	7.560 \pm 0.069	5.161 \pm 0.063	-0.203 \pm 0.094
2MASS J09432994-3833560	SpeX	3.441 \pm 0.056	5.142 \pm 0.053	3.320 \pm 0.051	-0.300 \pm 0.093
2MASS J10424135-2416050	SpeX	3.311 \pm 0.141	5.282 \pm 0.131	3.909 \pm 0.132	-0.180 \pm 0.277
2MASS J10542786-5431322	FIRE	3.877 \pm 0.123	5.706 \pm 0.102	3.819 \pm 0.099	0.343 \pm 0.079
2MASS J11155037-6731332	FIRE	4.825 \pm 0.097	7.314 \pm 0.080	4.664 \pm 0.075	0.396 \pm 0.075
2MASS J11231964-0509045	SpeX	2.622 \pm 0.063	4.720 \pm 0.061	3.171 \pm 0.058	0.044 \pm 0.102
2MASS J12294530+0752379	SpeX	4.014 \pm 0.054	6.307 \pm 0.052	3.985 \pm 0.049	-0.089 \pm 0.089
2MASS J13273095+0149384	SpeX	3.535 \pm 0.064	5.977 \pm 0.062	4.069 \pm 0.057	-0.071 \pm 0.091
2MASS J13313937-6513056	FIRE	7.371 \pm 0.132	9.545 \pm 0.112	6.990 \pm 0.104	0.029 \pm 0.079
2MASS J14230252+5146303	SpeX	4.252 \pm 0.078	6.056 \pm 0.075	5.097 \pm 0.070	-0.218 \pm 0.130
2MASS J14253465+2540050	SpeX	2.567 \pm 0.053	4.322 \pm 0.051	2.954 \pm 0.050	0.099 \pm 0.090
2MASS J16105843-0631325	SpeX	2.648 \pm 0.053	4.104 \pm 0.052	3.025 \pm 0.050	-0.038 \pm 0.088
2MASS J16210447-3711373	SpeX	4.515 \pm 0.074	6.130 \pm 0.071	4.477 \pm 0.064	0.028 \pm 0.095
2MASS J17120433-0323300	SpeX	2.641 \pm 0.051	4.758 \pm 0.050	3.301 \pm 0.046	0.161 \pm 0.085
2MASS J17364180-3425459	FIRE	2.848 \pm 0.095	5.225 \pm 0.079	3.073 \pm 0.074	-0.938 \pm 0.076
2MASS J17415439+0940537	SpeX	4.154 \pm 0.062	6.321 \pm 0.060	4.978 \pm 0.060	-0.120 \pm 0.102
2MASS J18365842-3507176	FIRE	4.078 \pm 0.152	6.527 \pm 0.126	4.920 \pm 0.116	-0.403 \pm 0.080
2MASS J18485108-8214422	FIRE	3.165 \pm 0.111	5.310 \pm 0.092	3.454 \pm 0.088	0.103 \pm 0.077
2MASS J18545092-5704417	FIRE	4.170 \pm 0.103	6.509 \pm 0.085	3.989 \pm 0.082	0.198 \pm 0.076
2MASS J19212977-2915507	SpeX	4.230 \pm 0.049	6.534 \pm 0.048	4.346 \pm 0.046	0.177 \pm 0.087
2MASS J19332754+2150009	SpeX	6.776 \pm 0.086	9.753 \pm 0.082	7.106 \pm 0.075	-0.082 \pm 0.104
2MASS J19395199-5750339	FIRE	4.120 \pm 0.169	5.766 \pm 0.140	4.439 \pm 0.126	0.182 \pm 0.081
2MASS J19544358+1801581	SpeX	3.808 \pm 0.061	6.072 \pm 0.059	4.776 \pm 0.055	0.530 \pm 0.088
2MASS J20125255+1246315	SpeX	4.482 \pm 0.080	5.156 \pm 0.077	4.380 \pm 0.067	0.046 \pm 0.104
2MASS J20291194+5750317	SpeX	2.849 \pm 0.065	4.247 \pm 0.065	2.997 \pm 0.061	0.157 \pm 0.101
2MASS J20495272-1716083	SpeX	3.344 \pm 0.097	5.198 \pm 0.092	3.281 \pm 0.088	0.046 \pm 0.129
2MASS J21010483+0307047	SpeX	3.350 \pm 0.097	5.210 \pm 0.092	3.271 \pm 0.088	0.047 \pm 0.129
2MASS J21265788+2531080	SpeX	6.955 \pm 0.083	10.580 \pm 0.078	6.898 \pm 0.072	-0.212 \pm 0.107
2MASS J21381698+5257188	SpeX	3.147 \pm 0.065	5.618 \pm 0.062	3.525 \pm 0.059	-0.050 \pm 0.106
2MASS J21513137-4017229	FIRE	3.348 \pm 0.094	5.135 \pm 0.078	3.319 \pm 0.074	0.236 \pm 0.076
2MASS J22244238+2230425	SpeX	2.734 \pm 0.092	4.871 \pm 0.089	3.525 \pm 0.083	-0.116 \pm 0.111
SPECULOOS-2	SpeX	1.466 \pm 0.052	2.860 \pm 0.052	1.993 \pm 0.051	-0.028 \pm 0.089
SPECULOOS-3	SpeX	3.335 \pm 0.080	5.760 \pm 0.076	3.436 \pm 0.072	0.070 \pm 0.100
LHS 3154	SpeX	2.233 \pm 0.069	3.687 \pm 0.069	2.993 \pm 0.065	0.232 \pm 0.097
TRAPPIST-1	FIRE	3.913 \pm 0.019	6.690 \pm 0.014	4.027 \pm 0.014	0.052 \pm 0.073
TRAPPIST-1	SpeX	4.566 \pm 0.084	6.891 \pm 0.073	4.618 \pm 0.067	0.052 \pm 0.073

- Gizis, J. E. 2002, *ApJ*, 575, 484, doi: [10.1086/341259](https://doi.org/10.1086/341259)
- Gonzales, E. C., Faherty, J. K., Gagné, J., et al. 2019, *ApJ*, 886, 131, doi: [10.3847/1538-4357/ab48fc](https://doi.org/10.3847/1538-4357/ab48fc)
- Gorlova, N. I., Meyer, M. R., Rieke, G. H., & Liebert, J. 2003, *ApJ*, 593, 1074, doi: [10.1086/376730](https://doi.org/10.1086/376730)
- Harris, C. R., Millman, K. J., van der Walt, S. J., et al. 2020, *Nature*, 585, 357, doi: [10.1038/s41586-020-2649-2](https://doi.org/10.1038/s41586-020-2649-2)
- Henry, T. J., & Jao, W.-C. 2024, *ARA&A*, 62, 593, doi: [10.1146/annurev-astro-052722-102740](https://doi.org/10.1146/annurev-astro-052722-102740)
- Henry, T. J., Jao, W.-C., Subasavage, J. P., et al. 2006, *AJ*, 132, 2360, doi: [10.1086/508233](https://doi.org/10.1086/508233)
- Henry, T. J., Jao, W.-C., Winters, J. G., et al. 2018, *AJ*, 155, 265, doi: [10.3847/1538-3881/aac262](https://doi.org/10.3847/1538-3881/aac262)
- Hoerl, A. E., & Kennard, R. W. 1970, *Technometrics*, 12, 55, doi: [10.1080/00401706.1970.10488634](https://doi.org/10.1080/00401706.1970.10488634)
- Hunter, J. D. 2007, *Computing in Science and Engineering*, 9, 90, doi: [10.1109/MCSE.2007.55](https://doi.org/10.1109/MCSE.2007.55)
- Joyce, R. R., Hinkle, K. H., Wallace, L., Dulick, M., & Lambert, D. L. 1998, *AJ*, 116, 2520, doi: [10.1086/300594](https://doi.org/10.1086/300594)
- Kirkpatrick, J. D., Cruz, K. L., Barman, T. S., et al. 2008, *ApJ*, 689, 1295, doi: [10.1086/592768](https://doi.org/10.1086/592768)
- Kirkpatrick, J. D., Looper, D. L., Burgasser, A. J., et al. 2010, *ApJS*, 190, 100, doi: [10.1088/0067-0049/190/1/100](https://doi.org/10.1088/0067-0049/190/1/100)
- Kleinmann, S. G., & Hall, D. N. B. 1986, *ApJS*, 62, 501, doi: [10.1086/191149](https://doi.org/10.1086/191149)
- Kolmogorov, A. N. 1933, *Giornale dell'Istituto Italiano degli Attuari*, 4, 83–91
- Kruskal, W. H., & Wallis, W. A. 1952, *Journal of the American Statistical Association*, 47, 583, doi: [10.2307/2280779](https://doi.org/10.2307/2280779)
- Lienhard, F., Queloz, D., Gillon, M., et al. 2020, *MNRAS*, 497, 3790, doi: [10.1093/mnras/staa2054](https://doi.org/10.1093/mnras/staa2054)
- Lodieu, N., Hambly, N. C., Jameson, R. F., & Hodgkin, S. T. 2008, *MNRAS*, 383, 1385, doi: [10.1111/j.1365-2966.2007.12676.x](https://doi.org/10.1111/j.1365-2966.2007.12676.x)
- Lucas, P. W., Roche, P. F., Allard, F., & Hauschildt, P. H. 2001, *MNRAS*, 326, 695, doi: [10.1046/j.1365-8711.2001.04666.x](https://doi.org/10.1046/j.1365-8711.2001.04666.x)
- MacDonald, J., & Mullan, D. J. 2017, *ApJ*, 850, 58, doi: [10.3847/1538-4357/aa9611](https://doi.org/10.3847/1538-4357/aa9611)
- Mann, A. W., Deacon, N. R., Gaidos, E., et al. 2014, *AJ*, 147, 160, doi: [10.1088/0004-6256/147/6/160](https://doi.org/10.1088/0004-6256/147/6/160)
- Martin, E. C., Mace, G. N., McLean, I. S., et al. 2017, *ApJ*, 838, 73, doi: [10.3847/1538-4357/aa6338](https://doi.org/10.3847/1538-4357/aa6338)
- McGovern, M. R., Kirkpatrick, J. D., McLean, I. S., et al. 2004, *ApJ*, 600, 1020, doi: [10.1086/379849](https://doi.org/10.1086/379849)
- Meyer, M. R., Edwards, S., Hinkle, K. H., & Strom, S. E. 1998, *ApJ*, 508, 397, doi: [10.1086/306402](https://doi.org/10.1086/306402)
- Mulders, G. D., Drażkowska, J., van der Marel, N., Ciesla, F. J., & Pascucci, I. 2021, *ApJL*, 920, L1, doi: [10.3847/2041-8213/ac2947](https://doi.org/10.3847/2041-8213/ac2947)
- Pedregosa, F., Varoquaux, G., Gramfort, A., et al. 2011, *Journal of Machine Learning Research*, 12, 2825, doi: [10.48550/arXiv.1201.0490](https://doi.org/10.48550/arXiv.1201.0490)
- Rayner, J. T., Cushing, M. C., & Vacca, W. D. 2009, *ApJS*, 185, 289, doi: [10.1088/0067-0049/185/2/289](https://doi.org/10.1088/0067-0049/185/2/289)
- Rayner, J. T., Toomey, D. W., Onaka, P. M., et al. 2003, *PASP*, 115, 362, doi: [10.1086/367745](https://doi.org/10.1086/367745)
- Reid, I. N., & Hawley, S. L. 2005, *New light on dark stars : red dwarfs, low-mass stars, brown dwarfs*, doi: [10.1007/3-540-27610-6](https://doi.org/10.1007/3-540-27610-6)
- Rojas-Ayala, B., Covey, K. R., Muirhead, P. S., & Lloyd, J. P. 2010, *ApJL*, 720, L113, doi: [10.1088/2041-8205/720/1/L113](https://doi.org/10.1088/2041-8205/720/1/L113)
- . 2012, *ApJ*, 748, 93, doi: [10.1088/0004-637X/748/2/93](https://doi.org/10.1088/0004-637X/748/2/93)
- Schneider, A. C., Greco, J., Cushing, M. C., et al. 2016a, *ApJ*, 817, 112, doi: [10.3847/0004-637X/817/2/112](https://doi.org/10.3847/0004-637X/817/2/112)
- . 2016b, *ApJ*, 817, 112, doi: [10.3847/0004-637X/817/2/112](https://doi.org/10.3847/0004-637X/817/2/112)
- Sebastian, D., Gillon, M., Ducrot, E., et al. 2021, *A&A*, 645, A100, doi: [10.1051/0004-6361/202038827](https://doi.org/10.1051/0004-6361/202038827)
- Sestovic, M., & Demory, B.-O. 2020, *A&A*, 641, A170, doi: [10.1051/0004-6361/202037732](https://doi.org/10.1051/0004-6361/202037732)
- Simcoe, R. A., Burgasser, A. J., Schechter, P. L., et al. 2013, *PASP*, 125, 270, doi: [10.1086/670241](https://doi.org/10.1086/670241)
- Smirnov, N. V. 1948, *Annals of Mathematical Statistics*, 19, 279–281
- Stefánsson, G., Mahadevan, S., Miguel, Y., et al. 2023, *Science*, 382, 1031, doi: [10.1126/science.abo0233](https://doi.org/10.1126/science.abo0233)
- Teegarden, B. J., Pravdo, S. H., Hicks, M., et al. 2003, *ApJL*, 589, L51, doi: [10.1086/375803](https://doi.org/10.1086/375803)
- Vacca, W. D., Cushing, M. C., & Rayner, J. T. 2003, *PASP*, 115, 389, doi: [10.1086/346193](https://doi.org/10.1086/346193)
- Virtanen, P., et al. 2020, *Nature Methods*, 17, 261–272
- Zechmeister, M., Dreizler, S., Ribas, I., et al. 2019, *A&A*, 627, A49, doi: [10.1051/0004-6361/201935460](https://doi.org/10.1051/0004-6361/201935460)